

Enabling mass manufacturing of industry-standard optical waveguide combiners

Stefan Steiner,^a Matthias Jotz,^b Frederik Bachhuber,^b Brian Bilenberg,^c
Tobias Hedegaard Bro,^c Alireza Rashed,^d Murat Deveci,^d Erhan Ercan,^e
Mariana Ballottin,^e and Jan Matthijs ter Meulen^{e,*}

^aLightTrans International GmbH, Jena, Germany

^bSCHOTT AG, Mainz, Germany

^cNIL Technology ApS, Kongens Lyngby, Denmark

^dOptoFidelity Oy, Tampere, Finland

^eMorphotonics B.V., Veldhoven, The Netherlands

ABSTRACT. Nanoimprinting of surface-relief grating-based waveguides has the potential to produce one of the industry-leading augmented reality (AR) smart glasses, but there are still many challenges in the design, scaling, and reproducibility of these imprinted waveguides. A promising path toward mass manufacturing of optical waveguide combiners is via large-area nanoimprinting. Here, we present the complete value chain with partners involved throughout the process: from design, mastering, and materials to imprinting and metrology, to prove that this method improves not only the manufacturing throughput but also the waveguide quality. We demonstrate that the replication and image quality are true to the intended design using large area, high refractive index ($n = 1.9$), square (300 mm \times 300 mm) glass substrates with high-refractive index resins ($n = 1.9$). This is shown to be valid for over 100 replications and for large area nanoimprinting (Gen5, 1100 mm \times 1300 mm). Our goal is to demonstrate a viable path toward high-volume and low-cost manufacturing of AR waveguides based on surface relief gratings.

© The Authors. Published by SPIE under a Creative Commons Attribution 4.0 International License. Distribution or reproduction of this work in whole or in part requires full attribution of the original publication, including its DOI. [DOI: [10.1117/1.JOM.3.3.033502](https://doi.org/10.1117/1.JOM.3.3.033502)]

Keywords: augmented reality; optical waveguides; nanoimprinting; mastering; high index glass; optical metrology; Metaverse

Paper 23002G received Feb. 28, 2023; revised Aug. 4, 2023; accepted Aug. 22, 2023; published Sep. 23, 2023.

1 Introduction

Presently, augmented reality (AR) is increasingly prevalent, being used to showcase products by companies in a range of industries. For example, automotive companies such as Volkswagen featured AR-based head-up-displays in their vehicles. Consumer electronics companies such as TCL, Vuzix, Sony, HTC, and Canon have also demonstrated their commitment to AR glasses by announcing new products in their AR/virtual reality (VR) portfolio. This growing market interest has only solidified our resolve as a consortium of companies to continue exploring the potential of high-volume and low-cost manufacturing of waveguides based on surface relief gratings (SRGs). Furthermore, it should be noted that it is important to consider the entire process flow from design to final waveguides to achieve the best performing waveguides.

In this paper, based on the proceedings of SPIE 2022 and 2023,^{1,2} we focus primarily on quality. We aim to demonstrate the replication fidelity and image quality data across the large Gen5-size format (1100 mm \times 1300 mm), as well as reproducibility over time. In addition,

*Address all correspondence to Jan Matthijs ter Meulen, jan.matthijs.ter.meulen@morphotonics.com

we are able to improve in quantity by producing 270 waveguides per imprint cycle on a Gen5-size substrate by tiling 9 individual 300 mm × 300 mm size, 1.9 refractive index glasses. Together, quality and quantity are required to meet the potential mass-market demand for cost-effective AR waveguides.

2 Waveguide Design

The design of the waveguide of the demonstrator was performed by LightTrans International. As a starting point, a well-known and understood basic layout was chosen: a so-called 1D-1D pupil expansion, which typically consists of three different grating regions [incoupler, exit pupil expander (EPE), and outcoupler, see Fig. 1]. As the name already implies, this particular approach is based on the separation of the directions of the pupil expansion into two different grating regions. While a uniformly distributed expansion of the light of the desired field of view (FoV) and the efficient transport of the light from incoupler to the demanded eye box are the main challenges of every waveguide design, in this approach the actual pupil expander grating is designed to multiply the pupil just in the x -direction and the outcoupler just in the y -direction (see Fig. 1). This separation of the pupil expansion allows for the utilization of 1D-periodic (so-called lamellar) grating structures for all mentioned grating regions, which enables a simpler design process as well as feasible and cost-efficient manufacturing. While this separation is the main advantage of this approach, it comes at the price of a limited maximum FoV. A larger angular spectrum of the light will require an increased extension of the expanding grating region, resulting in higher demands on the grating characteristics to achieve an acceptable uniformity.

After choosing a general design layout, its parameters (i.e., extension and shapes of the grating regions, as well as the required distances) can be calculated by geometrical considerations regarding the desired extent and position of the resulting eyebox. For this particular design task, the physical-optics software “VirtualLab Fusion” was used, which provides versatile tools for the design and analysis of such layouts and other complex waveguide systems. In the following step, the required grating periods can be determined according to the used wavelength, the refractive index of the substrate, and the desired FoV. In this work, we show an example design for 533 nm (with a Gaussian spectrum and a bandwidth of 60 nm) in combination with the desired FoV of $35^\circ \times 18^\circ$. Taking into account the refractive index of the intended glass substrate at 533 nm ($n = 1.9$, thickness: 1 mm), the grating periods were designed to 415 nm for incoupler and outcoupler, and 293.45 nm for the expansion grating. The latter value already includes the rotation of the grating lines by 45° in the plane of the substrate surface. To determine the required lateral extent of the outcoupler, the desired size of the eye box (15 mm × 8 mm) and the eye-relief must be taken into account (see Fig. 1).

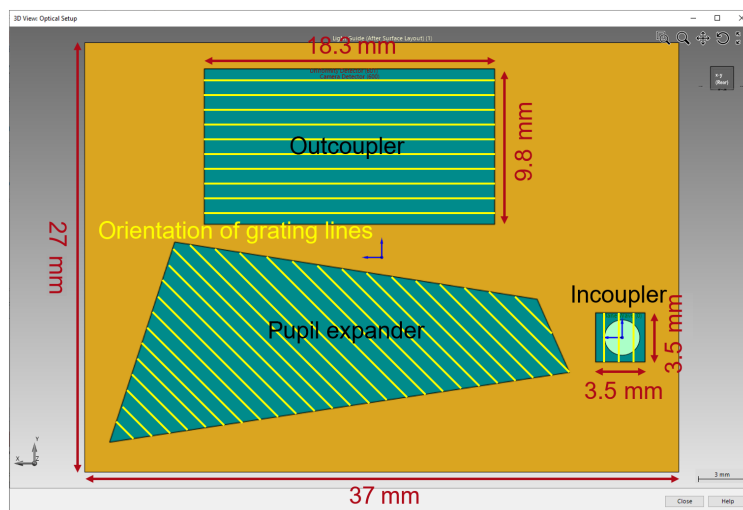


Fig. 1 Top view of the lateral layout of the designed waveguide. The orientations of the grating lines are indicated in green.

After setting proper extensions of all grating areas, the design of the specific grating structures was performed. For the incoupler, a blazed grating structure was chosen to enable a higher incoupling efficiency of the intended diffraction order ($T + 1$), due to the asymmetry of the structure. Furthermore, gratings with a binary shape were chosen as expansion and outcouple gratings, offering a good compromise between optical performance and feasible fabrication. As for the grating material, a high-refractive index resin was applied ($n = 1.88$ at 533 nm), which almost matches the index of the substrate and assures appropriately performing gratings.

To achieve a suitable optical performance, which usually means a good lateral and angular uniformity in combination with an adequate efficiency of the whole device, the diffraction efficiency in EPE and outcoupler must be controlled via a lateral variation of the grating parameters. For this purpose, smooth modulations of grating height and ridge width (respectively fill factor) were introduced for EPE and outcoupler. Regarding the desired direction of pupil expansion for each grating region, the modulation was configured horizontally (x -direction) for the EPE and vertically (y -direction) for the outcoupler (see Fig. 2) with a linear slope. This linear and continuous modulation allows for a distinct reduction of the free parameters in the optimization while not limiting the optical performance considerably.

In the next step, a parametric optimization was applied to determine the optimal set of parameters of the grating structures regarding the desired merit function. The following parameters were varied during this step: blaze angle of incoupler, height, and ridge width for EPE and outcoupler. As for the merit function, the lateral uniformity and efficiency were evaluated for 5 modes inside the desired FoV [central mode and one of each FoV quadrant ($\pm 11^\circ$, $\pm 5^\circ$)]. While the uniformity error should be as small as possible, the efficiencies of the different modes of the FoV are desired to be equal to provide a proper angular uniformity as well. The design and optimization steps were performed with the VirtualLab Fusion software, which enables a full-vectorial and accurate analysis of such complex waveguide systems by propagating electromagnetic waves. Moreover, the diffraction efficiencies of the gratings are calculated by rigorous coupled wave analysis, which also includes polarization effects during the light propagation inside the device. Due to the distinct sensitivity with respect to the polarization state of light for gratings in this range of structure size, the rigorous and local consideration for each individual interaction allows for very accurate modeling and design of the whole device.

The result of such optimizations usually exhibits a conflict between high efficiency and good uniformity, hence a design with good uniformity (mean uniformity error: 50.2%) and acceptable efficiency (mean efficiency per FoV mode: 0.8%) for the 5 FoV modes was chosen. The optimized grating parameters are shown in Table 1.

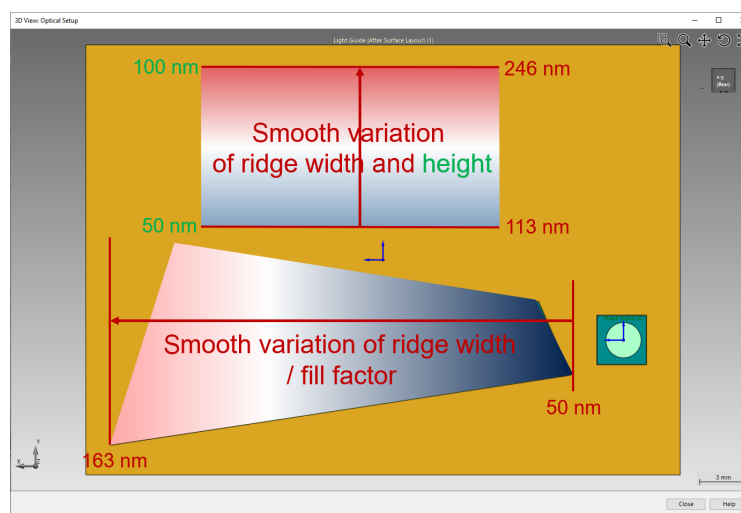


Fig. 2 Depiction of the modulation of grating parameters in the EPE and outcoupler with results obtained through parametric optimization.

Table 1 Overview of optimized grating parameters in the different regions of the designed waveguide.

	Period (nm)	Ridge width (nm)	Height (nm)	Blaze angle (deg)
Incoupler	415	415 (bottom)	203.1	29.9°
Pupil expander	293.45	50 to 163	50	—
Outcoupler	415	113 to 263	50 to 100	—

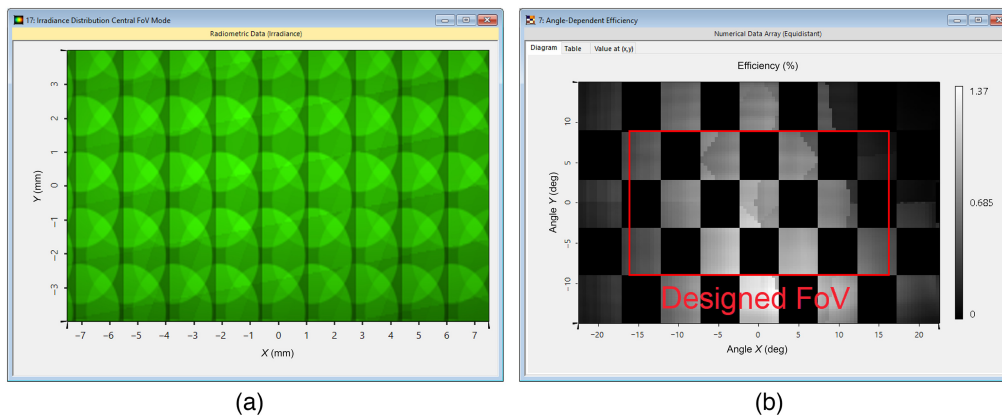


Fig. 3 (a) Irradiance distribution in the eyebox for the central mode of the FoV (0.86% efficiency, 20.2% lateral uniformity error) obtained by physical optics modeling in a real color view. (b) Angle-dependent distribution of the efficiency of the designed waveguide in the whole FoV (area of interest) and beyond, evaluated by a checkerboard pattern in angular coordinates (0.62% mean efficiency, 82.0% angular uniformity error).

The simulation results of the optimized system are shown in Fig. 3. The designed system exhibits a lateral uniformity error of 20.2% and an efficiency of 0.86% for the central direction of the FoV [see Fig. 3(a)]. Furthermore, the angle-dependent efficiency of the designed waveguide is assessed using a checkerboard pattern, where 1 rectangle has an angular extension of 5° by 6° [see Fig. 3(b)]. In the designed FoV, which is the area of interest, a mean efficiency of 0.62% with an angular uniformity error of 82% is obtained. According to the chosen design approach of a 1D-1D pupil expander, these are adequate values. A higher performance would be achievable by exchanging the gratings in incoupler and outcoupler: slanted grating profiles would offer more flexibility in the design but are more complex and expensive to manufacture.

3 Materials and Methods

3.1 Waveguide Master

The SRG waveguide master is made by NIL Technology in silicon by electron beam lithography (EBL) and dry etching. This approach is chosen for the master fabrication to ensure the highest possible quality of the SRGs. Figure 4(a) shows the final AR sub-master made in a UV replication process utilizing UV cured polymer on glass. As detailed in Fig. 4, a design with a binary pupil expander and output gratings and a blazed input grating was chosen to facilitate replication. The EBL is performed by a Jeol JBX-9500FSZ Gaussian-shaped 100 kV EBL tool. For the blazed input grating, a unique proprietary NIL Technology process is applied to ensure the highest possible quality of the blazed surfaces. The blazed grating period is defined by EBL, and the blazed grating is formed by dry etching. The binary pupil expander and multi-depth output gratings are defined by EBL and etched by multiple inductively coupled plasma etching cycles with additional lithography steps in between.

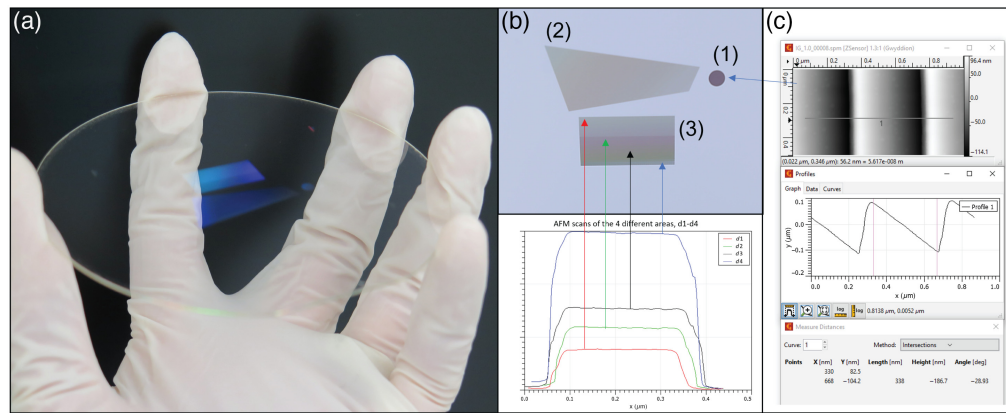


Fig. 4 (a) Final AR sub-master consisting of cured polymer on glass. (b) Top: (1) sub-master blazed input grating, (2) fill factor modulated pupil expander grating, and (3) depth and fill factor modulated output grating. Bottom: atomic force microscopy (AFM) scans of output grating showing both fill factor modulation from 17% (top) to 56% (bottom) and depth modulation from 72 (top) to 92 nm (bottom). (c) AFM scan of blazed input grating showing the sharp profile with 29° blaze angle, and 80° to horizontal anti-blaze angle.

The use of EBL to define all SRGs ensures a high accuracy of the grating periods and lateral dimensions while the use of dry etching to form the gratings in silicon ensures a high structure fidelity and precision of etch depths. After pattern transfer, the master is cleaned, and a first-generation sub-master is generated from the master by UV replication into a UV curable material on glass for subsequent recombination and fabrication of the waveguides.

The design parameters in the presented SRG waveguide are well within the fabrication rules of the silicon master as well as the replication process. NIL Technology is also able to produce more complex SRGs, such as slanted gratings and more advanced binary gratings. All these types of gratings can be combined on the master with total design freedom on relative placement and rotation of the individual gratings.

3.2 High-Refractive Index Glass

Glass is the backbone of SRG waveguides fabricated by nanoimprint lithography. SCHOTT RealView® wafers, typically circularly shaped with diameters of 100, 150, 200, or 300 mm and with a thickness between 0.3 and 1 mm, have been widely established in NIL manufacturing processes. They are available in a broad variety of refractive indices with index-matching resins, usually from 1.7 to 2.0. For applications in high-volume manufacturing, we demonstrated that it is possible to fabricate even larger square and rectangular wafers made from high-index glass that comply with the tight AR specifications. The substrates processed in this consortium are RealView® 1.9 wafers with the dimensions 300 mm × 300 mm × 1 mm.

The properties of the glass substrate play a crucial role for the performance of an AR device. First, the refractive index is a limiting factor for FoV. By maximizing transmission, optical losses due to absorption or scattering are minimized and fewer photons need to be generated to create the digital image. This helps to improve battery lifetime. A compact form factor and low weight have become very important particularly for those devices targeting the mass market. Weight can be directly influenced by material density and wafer thickness. However, reducing the thickness has a significant impact on the image quality as the number of bounces of the rays in the waveguide increases accordingly. More bounces correspond to higher risk of light losses and deflection by accumulation of angular errors. While the former affects the projector power consumption, the latter has an effect on image resolution and contrast. Hence, a very high flatness level is needed to meet the requirements of the AR industry.

The flatness on a global level is usually described by the total thickness variation (TTV) of the wafer. As a rule of thumb, it should be below 1 μm to produce high-performance waveguides for AR. Although TTV values tend to increase with larger substrate sizes, it is in fact the local thickness variation on an eye piece level that directly impacts the image quality of the AR device. Those values are well below 1 μm for any waveguide on the panel. Another rule of thumb states

that the surface roughness should be below 1 nm to avoid stronger scattering effects. This could also be realized for the panels.

Finally, there is the question how large those panels could potentially become. Technical flat and ultrathin glass has already been established in various fields of consumer electronics, such as display manufacturing, as it allows continuous large-area melting by overflow fusion or down-draw processes. The latter is comparably flexible with respect to different material compositions. The molten glass directly enters a hot-forming device, in which the glass is drawn through a nozzle into a large thin format. The resulting glass ribbon can be cut into sheets in-line. This is very cost-efficient, and panels with typical dimensions of 370 mm × 570 mm or 550 mm × 650 mm can be directly assessed. The hot forming process, however, requires glass types with a slow crystallization behavior, which is not the case for typical high-index glasses. Furthermore, TTV values are usually in a range of 5 μm . Even though this route does not seem to be an option now, it might become accessible to the AR industry through continuous innovation in the areas of high-index glass melting and TTV reduction.

The alternative is the optical glass route that provides access to a variety of high-index glasses. The melting process takes place in a melting tank with thoroughly controlled reaction conditions. This becomes particularly challenging with increasing refractive index of the target glass. The liquid glass is poured into strips and annealed. Those strips are drilled and sliced down into the desired format. By a well-elaborated lapping and polishing process, the wafers are brought into their final ultra-flat shape to meet the tough requirements of the AR industry.

Basically, the strip width obtained from the melting process is the limiting factor for one panel axis. As a matter of fact, with increasing refractive index, it becomes more demanding to produce strip widths >300 mm. The strip length is very flexible, but deviation from the square shape results in rising wafer flatness inhomogeneities from the lapping and polishing process. The present 300 mm × 300 mm substrates already shows the potential of the technology and, with further development of the lapping and polishing process, larger rectangular substrates seem to be accessible.

3.3 High-Refractive Index Resin

For AR waveguides, the replications are made using a high-refractive index resin to match the high-refractive index glass to obtain the highest FoV. This solvent-free resin has been co-developed and supplied by Pixelligent (Pixelligent PixNIL SFT1). The refractive index is 1.89 at a wavelength of 550 nm, with a viscosity of 575 cP. The transmission of a 12 μm thick layer is over 94% with a very low haze. The refractive index of the PixNIL SFT1 has not yet been fine-tuned to the refractive index of the Schott glass. The uniformity of the obtained nanoimprints is discussed in the results section.

3.4 Large Area Nanoimprinting

To ensure mass manufacturing at high accuracy, roll-to-plate (R2P) NIL technology was used at Morphotonics. In the R2P nanoimprinting system, a transparent flexible stamp containing the desired inversed texture is mounted around rollers; these rollers guide the flexible stamp. The UV curable resin is then dispensed onto a substrate using jet dispensing, and subsequently pressed under the flexible stamp and rollers. The resin is cured using a UV light source (365 nm), and the flexible stamp is delaminated from the substrate. In this way, the pattern is imprinted on the substrate. The advantage of this imprint technology is its scalability to larger substrate sizes, beyond wafer-scale, while maintaining good replication fidelity (preserved texture shape) and dimensional stability (no track pitch variation). Multiple rigid wafers can be imprinted in one pass, each containing a multiple-up of products adjacent to each other. Hereby, mass volume production is enabled.

The process starts with the scaling of the sub-master, containing one waveguiding eye-piece, to a scaled-up sub-master. With the Morphotonics proprietary upscaling process, an array of waveguiding eye-pieces is made. In this demo effort, the squared upscaled sub-master contains 6 rows of each having 5 eyepieces for a total of 30 eyepieces, as shown in Fig. 5. Height variations between the different waveguiding products as well as the height and width of the seam in between the different waveguiding products have to be tightly controlled. Height variations result in a varying imprint pressure close to the seam. With the controlled Morphotonics' upscaling

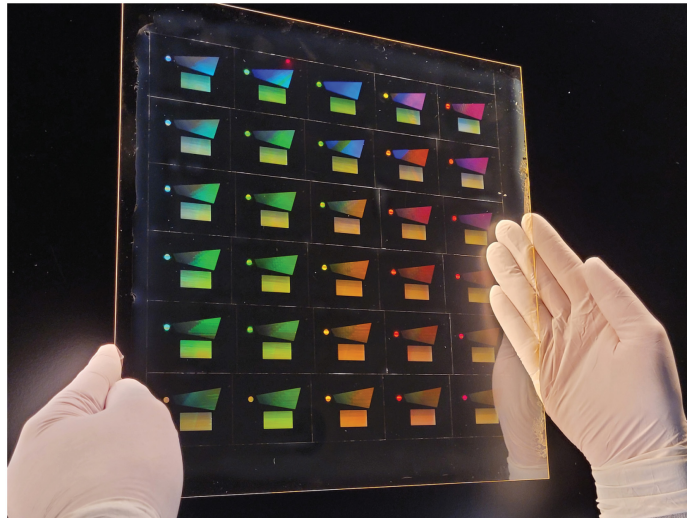


Fig. 5 Imprint from the 30-up sub-master.

process, the area next to the seam with deviations in imprint quality is minimized to a few millimeter. This small “bleeding” area is outside the active area and is removed in the singulation of the eye-pieces.

The flexible stamp used in the large-area R2P imprint steps can contain multiple scaled-up sub-master areas, imprinting on multiple wafers placed on a carrier. In this work, the replication is made on a square 300 mm × 300 mm wafer. With the use of the Morphotonics Portis NIL600 imprint module, handling up to 600 mm × 800 mm substrates, 4 wafers can be imprinted in 1 imprint cycle. The Morphotonics Portis NIL1100 can imprint up to a size of 1100 mm × 1300 mm, containing 9 wafers on a carrier.

In the replication process, there are several key parameters such as the re-usability of the flexible stamp, the dimensional stability, the replication fidelity into resins with high refractive index, and the layer thickness uniformity.

The re-usability of the flexible stamp is important to ensure a reproducible process at lowest costs. Each imprint having the same imprint quality limits the quality control step significantly. The Morphotonics flexible stamps have a re-usability of more than 500 times, proven in volume production with different customers. In addition, the stamps must ensure dimension stability. The track pitch of the different optical elements must remain constant within an imprint as well among different imprints. The flexible stamp is not allowed to be stretched due to the applied forces or thermal or humidity changes. To ensure this dimensional stability, Morphotonics uses a flexible stamp, that is, a composite foil with excellent physical properties, such as a thermal expansion coefficient of 5 ppm/°C, a hygroscopic expansion <1 ppm/%RH, and a Young’s modulus >20 GPa. Here, we call this a high dimension stability flexible stamp.

3.5 Metrology

The fabrication quality of the replicated samples is evaluated with two complementary measurement methods at Optofidelity: image quality measurement and a Littrow diffractometer. Littrow measurements provide direct feedback regarding the homogeneity and reproducibility of the fabrication process.^{3,4} With this method, one can precisely measure the grating period and relative orientation of grating lines.

On the other hand, image quality measurements can be used to assess the optical functionality of the replicated waveguides. For the end user of an AR device, the image quality produced by the waveguide is naturally the most important part of the user experience. The accuracy of the fabrication process can ensure such demanded image quality. In this work, checkerboard contrast ratio and luminescence uniformity of the diffractive waveguides are evaluated and compared. Furthermore, modulation transfer function (MTF) measurement is used as another tool to assess the optical performance of the replicated samples.⁵⁻⁸ This method provides a precise and

quantitative measure of resolution in waveguides and help manufacturers pinpoint subtle differences in fabrication quality.

3.5.1 Littrow diffractometer measurements

A Littrow diffractometer is used to evaluate the fabrication uniformity by measuring the grating period and relative orientation of the grating lines. This is done by determining the so-called Littrow angle of the grating. For achieving an optimal performance of diffractive waveguide gratings, it is necessary to have very high accuracies in the fabrication of the period and orientation of the grating. That is why, the Littrow diffractometer of Optofidelity is designed and calibrated to measure with an accuracy in the scale of picometers and arcseconds reliably and repeatably.

Our lab setup is equipped with a very stable and high-quality collimated laser beam, operating at 405 nm wavelength. The laser beam is pointed to the sample, and the sample surface is calibrated to be perpendicular to the laser beam. This is checked by placing a beam splitter directly in front of the laser beam and using a monochrome camera to see the reflected beam in the center of the sensor. For controlling yaw and roll of the sample, we are using two very high-accuracy rotary stages on top of each other. These stages are used to move the sample until we get a Littrow diffracted beam back to the sensor. Consequently, we can calculate the period of the grating using the diffraction equation

$$2d \sin \alpha = m\lambda, \quad (1)$$

where d is the grating period, α is the yaw angle of the rotary stage, m is the diffraction order, and λ is the laser beam's wavelength. In the Littrow configuration, the grating lines will be vertical, so the roll stage directly gives the relative grating angle. Because one measurement is done at a specific location on the grating, also the XY-stage is used to move the laser. This enables us to measure any point on the grating or the whole grating area, which is usually the most beneficial way to characterize the grating uniformity. However, this method is time-consuming because measurements are done in a single location at a time. Therefore, the larger the grating area or denser the sample rate, the more time it will cost. That is why, the Littrow diffractometer is mainly used to measure the master before replication and the produced replicas that have failed the image quality test, though it can also be used to test reproducibility and uniformity of random samples.

3.5.2 Image quality measurements

We evaluated homogeneity and reproducibility of the fabricated diffractive waveguides by performing image quality measurements. To do this, we project a test pattern through the waveguide, and using image processing methods, we analyze the checkerboard contrast ratio and luminescence uniformity of the waveguide. The projection should be done by a reference light engine. Typical pico-projectors used in commercial headsets are not the best choice for characterizing the waveguides, as they typically suffer from a lack of stability, uniformity, and/or contrast. A stable and uniform light source with high contrast and low distortion optics as well as a large FoV is required for an accurate metrology.

A standard WG-IQ tester, designed and developed by OptoFidelity, is used to characterize the target samples. This tester can characterize diced and wafer-based waveguides in both transmission and reflection modes at desired wrap angles and pantoscopic tilts. A uniform light engine (OptoProjector) of the tester is used to project test patterns with a maximum FoV of $72^\circ \times 42^\circ$. The projection lens, OptoEye 2.0 by OptoFidelity, images the reticles to infinity and also creates an external exit pupil for illuminating the input grating of the waveguide. It is equipped with a motorized iris which makes the exit pupil diameter adjustable from 1 to 3 mm. Furthermore, the included motorized polarizer of the lens gives us the opportunity to set the polarization state of the projected light at a desired angle between -180° and $+180^\circ$.

The used test patterns are solid and checkerboard reticles with FoV of $45^\circ \times 30^\circ$. They are printed on a diced piece of glass substrate using a photomask lithography method. These reticle patterns are pre-distorted to compensate for the distortion of the projection lens and therefore

form a non-distorted image at infinity. The light passed through the diffractive waveguide is detected after the outcoupler grating in the eyebox of the waveguide by another OptoEye 2.0 lens. However, this lens is without a polarizer, and it has a fixed iris. Like the OptoProjector lens, the output OptoEye 2.0 lens is focused into infinity. This lens comes with a 3 mm external entrance pupil, mimicking the average human pupil size, and can be moved to scan the eyebox of the waveguide. The large 100° diagonal FoV of this lens allows us to see the full image of the test pattern without mechanical tilting of the camera. Both projector and camera lens optical axes are placed normal to the waveguide over the input and output couplers, respectively. The projected image of the reticle on a monochromatic camera sensor is measured with and without the waveguide and analyzed to assess waveguide image quality.

The designed waveguides for this study have a FoV of $32^\circ \times 18^\circ$, which is smaller than the FoV of our standard test patterns ($45^\circ \times 30^\circ$). Our analyses are done in the region of interest which is the FoV of the replicated waveguides [Fig. 3(b)]. Note that this can have a detrimental effect on the results, especially for contrast, as our illumination angles exceed the design specifications of the waveguides. However, for analyzing the homogeneity of the sample set, this should have no influence. The problem could be avoided by designing a custom reticle for these samples.

The test waveguides were carefully positioned with respect to the projector and camera to achieve repeatable and reliable results. The input grating is centered at the 3 mm exit pupil of the OptoProjector. A green LED (with a central wavelength of 523 nm and FWHM of 26 nm) is used for lighting as the waveguide is optimized to work at that spectral range. The camera OptoEye lens is placed in the transmission mode at the waveguide's eyebox center within an eye relief distance of 5 mm.

3.5.3 MTF measurements

The industry-standard way of quantifying the achievable imaging resolution of an optical system, for example, a camera lens, is the so-called MTF. It is a measure of the ability of a system to reproduce fine spatial details, with higher values indicating higher image quality.

In the context of AR devices, MTF measurements are essential because they provide a quantitative assessment of how well the device can display objects requiring high angular resolution, such as text or small graphics. This is essential for ensuring that the AR content being displayed is clear and easy to read or interpret for the user. In an AR headset, it is desirable that the projected image has a similar resolution as the projector. However, even slight imperfections in the glass waveguide or the diffractive gratings can also cause stray light, ghosting, and other effects that can severely limit the MTF performance of the headset. Given the extremely low tolerances of the gratings for fabrication errors, accurately assessing the MTF of the waveguides is critical.

MTF measurement systems typically use small FoV collimators to project test patterns with very high angular resolution through the tested optical system. Multiple collimators or tilting mechanics are needed to investigate a range of incidence angles. The test patterns, often a cross or slanted rectangles, are imaged on the other side of the tested system using cameras with telescope objectives. The collimators and telescopes are as close to the diffraction limit as possible to ensure that the measurement system is not limiting the resolution. The measurements are typically repeated at multiple wavelengths to assess the spectral performance.

Measuring the MTF of AR waveguides requires careful consideration in the implementation of the optical system. The significant difference is the requirement of pupil matching, as the projector exit pupil needs to be at the input grating of the waveguide, and correspondingly the camera input pupil must be placed in the eyebox where the user's eye would be. Also, some waveguides are designed to work in reflection mode, requiring that the camera and the projector are placed on the same side of the waveguide, which can cause mechanical difficulties.

Our measurement setup is designed specifically for AR waveguides. The sample can be mounted at an arbitrary angle between a collimator and a telescope. An adjustable iris controls the projected exit pupil size to match the input grating of the waveguide. The central wavelength of the illuminating LED is 530 nm. The setup uses a negative crosshair reticle to produce target lines (horizontal and vertical), which are used to calculate the MTF. The effective focal lens of

the collimator is 152 mm, and the beam diameter was set to 2 mm. The beam was focused on the incoupler side (input grating). After the perpendicular alignment of the waveguide, the beam was collected from the outcoupler (eyebow) on the opposite side of the waveguide. The image of the reticle is formed on the monochrome camera sensor. This image is processed, and MTF is calculated for the various frequencies.

4 Results and Discussion

Waveguide imprints were made with R2P technology using the upscaled sub-master, high-refractive index glass and resin. Two types of run of imprints were performed, which here we call homogeneity and reproducibility runs. In a homogeneity run, the goal is to show that quality is kept over a large area imprint. In a Gen5 area, we show that it is possible to imprint on 9 square wafers (300 mm × 300 mm), with 30 waveguides each, on 1 imprint cycle. This corresponds to 270 waveguides imprinted in 1 machine cycle (see Fig. 6).

Furthermore, in a reproducibility run, the goal is to ensure that using the same flexible stamp, the quality is kept over multiple imprints. Here, more than 100 runs were performed using a flexible stamp made from a 30-up upscaled sub-master (Fig. 5).

We measured waveguides from the two different groups of samples, the homogeneity (H1 to H3) and reproducibility (R1 to R6) test waveguides (see Fig. 7). Their quality was assessed by structural and functional tests.

To assess the replication fidelity of the samples, we measured with a Littrow diffractometer the input, pupil expander, and output gratings for the nine different samples. In total, 45 points on the outcoupler grating, 47 points on the expander grating, and 5 points on the incoupler grating were measured to get an optimal sample rate, but also managing strict time constraints. Examples of one outcoupler period measurements have been shown in Fig. 8.

The average period with standard deviation and standard deviation of the relative orientation for each grating are shown in Fig. 9. From these results, we can conclude that the uniformity for all the gratings is excellent. For example, the designed grating period for the outcoupler was 415 nm and 90° for the orientation. We measured the average of the outcoupler grating period to be 414.99 nm with the standard deviation being ± 20 pm and the relative orientation standard

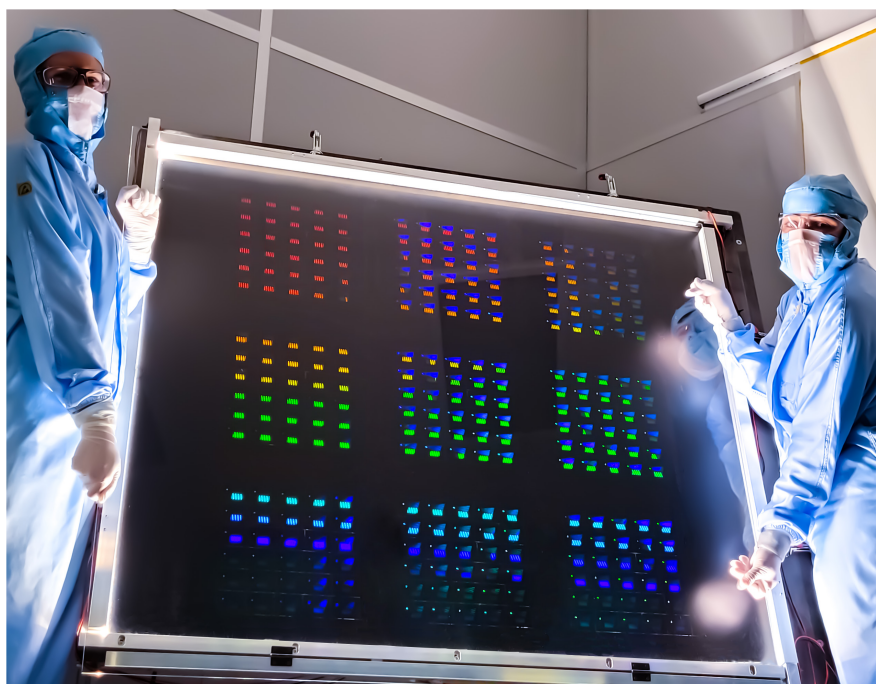


Fig. 6 Replication of the 30-up scaled-up sub-master on 9 single wafers producing 270 waveguides in one imprint pass.

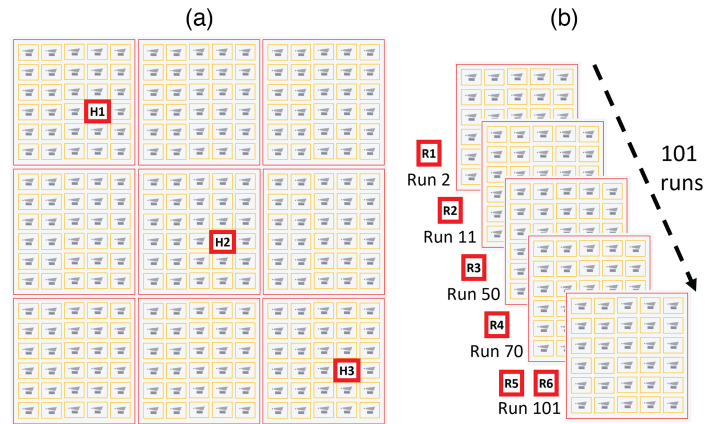


Fig. 7 (a) Homogeneity (H1 to H3) and (b) reproducibility (R1 to R6) test waveguides.



Fig. 8 Example of outcoupler grating period uniformity for one sample.

deviation to be ± 5 arcsec. This implies that the manufacturing process is very high quality, and the reproducibility is excellent for high-volume production.

Uniform imprints, without variations in residual layer thickness, are required for the best contrast and lowest waveguide losses. The thickness of the residual layer is determined by the imprint process and resin characteristics. The lowest layer thickness variation is achieved with the lowest residual layer thickness. With the current solvent-free high-refractive index resin, a layer thickness of around $4.6 \mu\text{m}$ is obtained. Further development in solvent-free high-refractive index resin with lowered viscosity is needed to achieve minimal residual layer thicknesses.

The analysis results of the checkerboard contrast for both sample groups of the homogeneity (H1 to H3) and reproducibility (R1 to R6) test waveguides are shown in Fig. 10(c). The checkerboard contrast is calculated by analyzing the detected checkerboard image at the center of the eyebox of the waveguide. First, the dark current of the camera sensor is subtracted. By dividing the gray level of the center white square by the average gray level of the surrounding black squares, one can calculate the local checkerboard contrast of the illuminated waveguides. The very high inherent contrast value of the OptoProjector (180:1) guarantees a reliable contrast measurement for the designed waveguides. The insignificant fluctuation of the contrast values

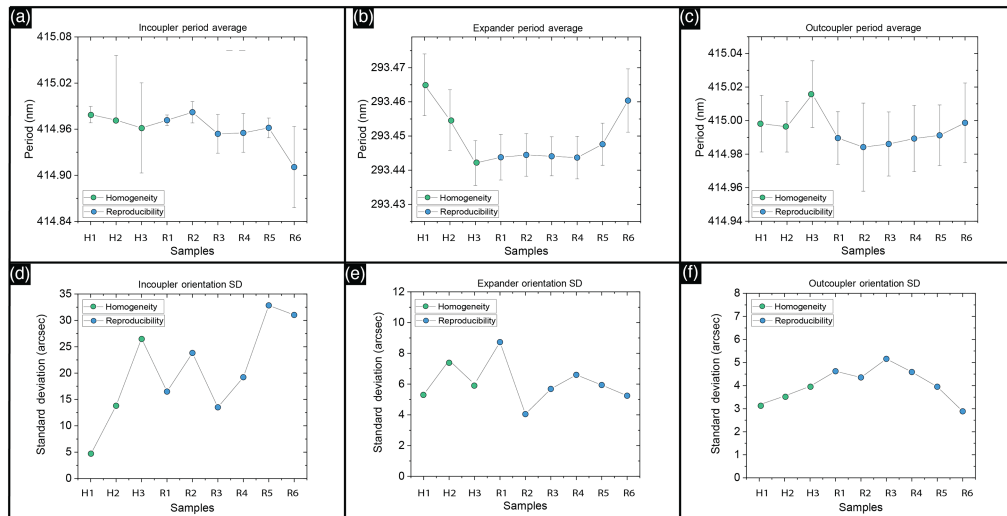


Fig. 9 (a)–(c) Average period with standard deviation of each grating. The graph shows that the average period is similar from sample to sample. (d)–(f) Standard deviation of the relative orientation of the grating lines. Incoupler SD presents a low reliability due to small number of measurement points.

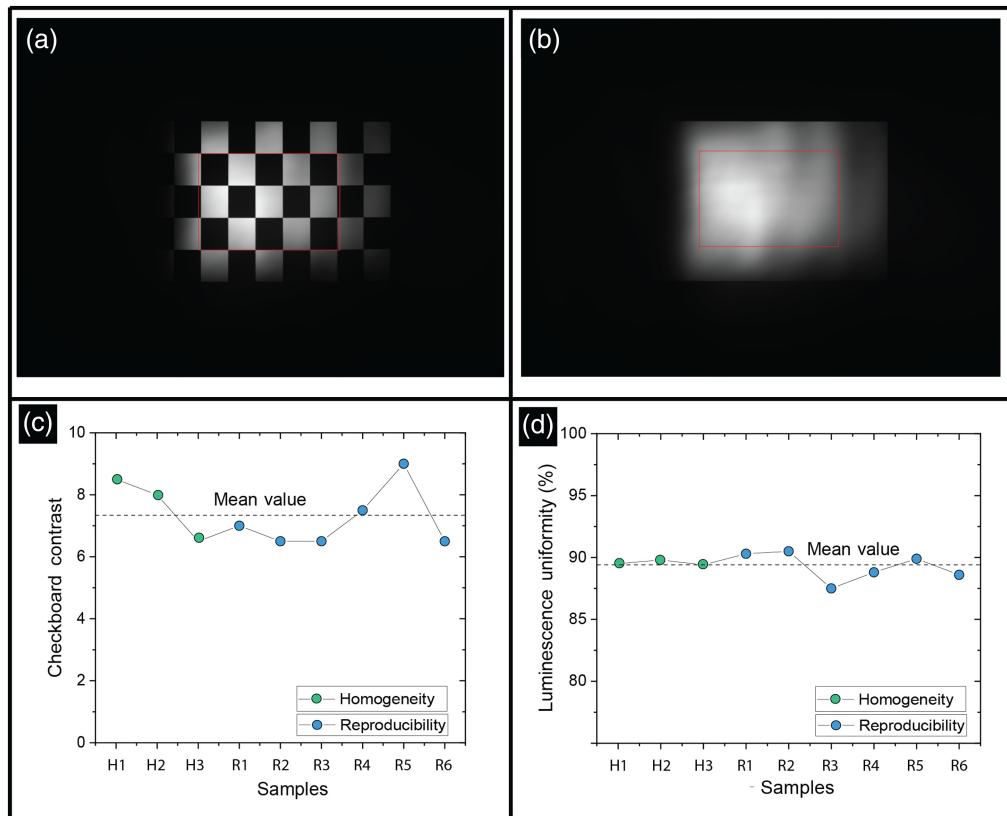


Fig. 10 Regions of interest for analyzing the waveguide images based on the FoV of the test waveguides are shown as a red frame for both (a) checkerboard and (b) solid reticles. For both groups of the homogeneity (H1 to H3) and reproducibility (R1 to R6) waveguides, the analysis results of the checkerboard contrast and luminescence uniformity are presented in panels (c) and (d), respectively.

around their mean value for both groups of the test waveguides confirms the presence of homogeneity and reproducibility in the replication process.

Typically, the largest challenge for diffractive waveguides is luminance uniformity. Any imperfection in the fabrication process can result in a remarkable quality drop in the luminance uniformity of the diffractive waveguide. Therefore, the assessment of this parameter can be considered a qualitative assessment for the fabrication process. In this study, the luminescence analysis is done based on IEC 63145 standard using 13 spots distributed across the waveguide FoV in an ANSI13 pattern.⁹ The luminance value for each spot with the same area is the average luminance. The projecting system should have a very high uniformity to validate the achieved qualitative analysis based on this approach. Our designed OptoProjector provided uniformity values higher than 96% at the FoV range of the waveguide. The analysis reports the luminescence nonuniformity in terms of a percentage. Then, the luminescence uniformity is calculated based on the acquired nonuniformity

$$\text{Luminescence uniformity (\%)} = 100 (\%) - \text{luminescence nonuniformity (\%)}. \quad (2)$$

The nonuniformity is calculated based on the acquired normalized luminescence mean value deviation of the selected 13 spots from their averaged maximum luminescence value

$$\text{Nonuniformity (\%)} = \left[\frac{\text{max luminance} - \text{mean luminance}}{\text{mean luminance}} \right] \times 100 (\%). \quad (3)$$

Figure 10(d) shows the evaluated uniformity of both groups of the test waveguides and compares the calculated values with their mean value. As is evident in this figure, the negligible fluctuations of this parameter from the mean value for the homogeneity waveguides (H1 to H3) confirm the expected fabrication uniformity of the diffractive waveguides. On the other hand, a very slight difference between the uniformity of R1 to R3 samples and their mean value validates the existing replication in the physical and optical properties of the fabricated waveguides.

Both the checkerboard contrast and luminescence uniformity results are supportive evidence for the presented Littrow measurement results and, consequently, for the accuracy, repeatability, and reproducibility of the proposed large-area waveguide fabrication method.

The results of the MTF measurements for all samples versus spatial frequency (cycles/mm) are shown in Fig. 11(a), and the MTF values for 40% contrast are shown in Fig. 11(b). In Fig. 11(a), MTF graphs show a good agreement between all samples of H1 to R4. In other words, not only do tiles in single imprints for H1 to H3 show a close correlation of MTF values but also the reproducibility of imprints is closely correlated. In R5 and R6, a slight decrease in MTF can be seen, possibly related to minor reproducibility issues after 100 imprints. In Fig. 11(b),

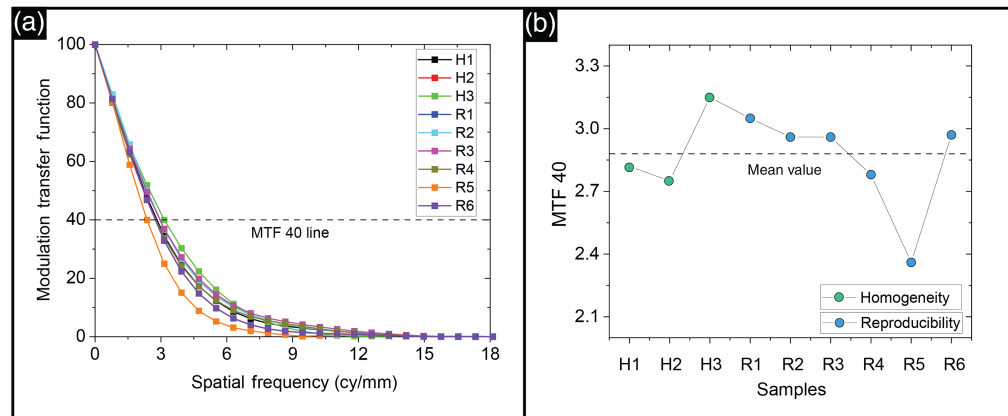


Fig. 11 (a) MTF graphs for all samples versus spatial frequency, H1 to H3 are selected tiles from single imprint number 1, and R1 to R6 are imprints 2, 11, 50, 70, and 101. (b) MTF of 40% is shown for all imprints and tiles for a closer comparison.

the spatial frequency where MTF drops to 40% is shown for all imprints and tiles for a more detailed comparison.

The results in this paper arise from a combined effort of pioneering partners with limited time for optimization. The production chain has not been adjusted for deviations in the master process, sub-master up-scaling process or the different replication steps, nor have the materials used been fully optimized. For example, the texture height has only been corrected by approximation for the shrinkage of the resin. With further optimization, waveguides with even better performance could be realized.

5 Conclusion

We have demonstrated in this paper that for a successful transition to high-volume manufacturing of AR waveguide optics, a display-oriented, high-quality focused, large-area manufacturing mindset is not only needed but is also already available. The array of high-index squared glass enables the increase in production volume of AR waveguide optics. Together with the complex design, the high-end mastering and the in-depth quality inspection capabilities available, the reproducible large-area nanoimprinted demo proves that the mass production route is feasible.

An end-to-end supply chain and cooperation between different disciplines is also key. As a consortium of pioneers, we were able to iterate based on a robust design, excellent mastering, using unprecedented materials and proven large-area nanoimprinting, topped with the unique metrology capabilities. We hope this exemplary work will inspire the industry to take the necessary steps to help fulfill the promise of smart glasses.

Disclosures

The authors declare no conflict of interest.

Data Availability

Datasets generated during the current study are available from the corresponding author on reasonable request.

Acknowledgments

The authors would like to thank their colleagues for their support of this work, with special thanks to Jesper Leppinen, Farhad Ghasemzadeh from OptoFidelity, Daniëlle van der Heijden, Bodine van der Lubbe, Rana Al-Amidi, Pim Veldhuizen, Andrea Scheidegger, Nico Jansen, and Lauréline Seurre from Morphotonics.

References

1. M. Jotz et al., "The path towards mass manufacturing of optical waveguide combiners via large-area nanoimprinting," *Proc. SPIE* **11931**, 1193109 (2022).
2. S. Steiner et al., "Enabling the Metaverse through mass manufacturing of industry-standard optical waveguide combiners," *Proc. SPIE* **12449**, 1244906 (2023).
3. E. Popov, L. Tsonev, and D. Maystre, "Gratings: general properties of the Littrow mounting and energy flow distribution," *J. Mod. Opt.* **37**, 367 (1990).
4. Y. Wu et al., "Design of ultra-compact augmented reality display based on grating waveguide with curved variable-period grating," *Opt. Commun.* **529**, 128980 (2023).
5. E. Eisenberg and J. Jensen, "Measuring and qualifying optical performance of AR/VR/MR device displays and addressing the unique visual requirements of transparent AR/MR displays," *Proc. SPIE* **11310**, 113100S (2020).
6. T. L. Williams, *The Optical Transfer Function of Imaging Systems*, Routledge (2018).
7. J. T. Dobbins, III, "Image quality metrics for digital systems," in *Handbook of Medical Imaging*, R. L. Van Metter, J. Beutel, and H. L. Kundel, Eds., Vol. **1**, pp. 161–222, SPIE Press (2000).
8. C. S. Williams and O. A. Becklund, *Introduction to the Optical Transfer Function*, Vol. **112**, SPIE Press (2002).
9. W. O. Davis, M. Beard, and R. Jackson, "Trajectory precision of micromachined scanning mirrors for laser beam scanning pico-projector displays," *Proc. SPIE* **8252**, 825203 (2012).

Stefan Steiner is a principal scientist at LightTrans International GmbH from Jena, Germany, working on optical modeling and design with LightTrans' fast physical-optics software "VirtualLab Fusion." He received his diploma in physics from Friedrich-Schiller University Jena, Germany, in 2008, where he conducted research on low-temperature physics. Later, he received his PhD in optical micro structure design and technology from the Institute of Applied Physics, Jena, Germany, in 2015. He is a member of SPIE.

Biographies of the other authors are not available.